HHS Public Access

Author manuscript

Radiat Res. Author manuscript; available in PMC 2021 September 16.

Published in final edited form as:

Radiat Res. 2020 September 16; 194(3): 277–287. doi:10.1667/RADE-20-00051.1.

Non-Human Primates Receiving High-Dose Total-Body Irradiation are at Risk of Developing Cerebrovascular Injury Years Postirradiation

Rachel N. Andrews[a,b,c,1], **Ethan G. Bloomer**[d], **John D. Olson**[b], **David B. Hanbury**[e], **Gregory O. Dugan**[b], **Christopher T. Whitlow**[c,f,g,h], **J. Mark Cline**[b]

[a]Department of Radiation Oncology, Section of Radiation Biology, Wake Forest School of Medicine, Medical Center Boulevard, Winston-Salem, North Carolina 27157;

[b]Department of Pathology, Section on Comparative Medicine, Wake Forest School of Medicine, Medical Center Boulevard, Winston-Salem, North Carolina 27157;

[c]Department of Wake Forest Baptist Comprehensive Cancer Center, Wake Forest School of Medicine, Medical Center Boulevard, Winston-Salem, North Carolina 27157;

[d]University of Florida, College of Veterinary Medicine, Gainesville, Florida 32608;

[e]Department of Psychology, Averett University, Danville, Virginia 24541;

[f]Department of Radiology, Section of Neuroradiology, Wake Forest School of Medicine, Medical Center Boulevard, Winston-Salem, North Carolina 27157

[g]Department of Biomedical Engineering, Wake Forest School of Medicine, Medical Center Boulevard, Winston-Salem, North Carolina 27157

[h]Department of Biostatistics and Data Science, Wake Forest School of Medicine, Medical Center Boulevard, Winston-Salem, North Carolina 27157

Abstract

Nuclear accidents and acts of terrorism have the potential to expose thousands of people to high-dose total-body iradiation (TBI). Those who survive the acute radiation syndrome are at risk of developing chronic, degenerative radiation-induced injuries [delayed effects of acute radiation (DEARE)] that may negatively affect quality of life. A growing body of literature suggests that the brain may be vulnerable to radiation injury at survivable doses, yet the long-term consequences of high-dose TBI on the adult brain are unclear. Herein we report the occurrence of lesions consistent with cerebrovascular injury, detected by susceptibility-weighted magnetic resonance imaging (MRI), in a cohort of non-human primate [(NHP); rhesus macaque, *Macaca mulatta*] long-term survivors of high-dose TBI (1.1–8.5 Gy). Animals were monitored longitudinally with brain MRI (approximately once every three years). Susceptibility-weighted images (SWI) were reviewed for hypointensities (cerebral microbleeds and/or focal necrosis). SWI hypointensities were noted in 13% of irradiated NHP; lesions were not observed in control animals. A prior history of exposure was correlated with an increased risk of developing a lesion detectable by MRI ($P = 0.003$).

[1]Address for correspondence: Department of Radiation Oncology, Section of Radiation Biology, Wake Forest University School of Medicine, Medical Center Blvd., Winston-Salem, NC 27157; rnandrew@wakehealth.edu.

Twelve of 16 animals had at least one brain lesion present at the time of the first MRI evaluation; a subset of animals (n = 7) developed new lesions during the surveillance period (3.7–11.3 years postirradiation). Lesions occurred with a predilection for white matter and the gray-white matter junction. The majority of animals with lesions had one to three SWI hypointensities, but some animals had multifocal disease (n = 2). Histopathologic evaluation of deceased animals within the cohort (n = 3) revealed malformation of the cerebral vasculature and remodeling of the blood vessel walls. There was no association between comorbid diabetes mellitus or hypertension with SWI lesion status. These data suggest that long-term TBI survivors may be at risk of developing cerebrovascular injury years after irradiation.

INTRODUCTION

Acts of nuclear terrorism and incidents involving nuclear power reactors have the capacity to expose hundreds of thousands of people to potentially harmful doses of radiation (1). Radiation exposure in these scenarios is presumed unavoidable. Patients who survive the acute radiation syndrome (ARS) and those receiving lower doses of radiation may be at risk of developing delayed effects of acute radiation exposure (DEARE), comprised of a myriad of degenerative and inflammatory conditions affecting multiple organs, and with negative effect on quality of life (2). Thus there is a profound need to understand the long-term health effects of such radiation exposures to enable adequate risk assessment and direct patient follow-up and management practices.

The brain is considered radioresistant, with single dose total-body irradiation (TBI) of 20–50 Gy required to induce acute radiation syndrome (ARS) of the central nervous system (3). However, a growing body of literature suggests that the brain may be vulnerable to injury at lower doses (4–18). Retrospective analyses of atomic bomb survivors indicate that low-dose *in utero* radiation exposure (≥0.06 Gy at 8–15 weeks' gestation and ≥0.28 Gy 16–25 weeks' gestation) may result in dose-related reduction in cognitive function, microcephaly and seizures (19–24). Neurocognitive impairment may also occur in children receiving myeloablative doses of TBI for hematopoietic cell transplantation (25–32). Studies evaluating the long-term ramifications of single-dose TBI on the adult brain have been limited; however, retrospective analyses of long-term radiation survivor cohorts indicate survivors may have increased risk of stroke and vascular encephalopathy (13–15).

Studies evaluating the long-term effects of radiation in humans are confounded by factors that include socioeconomic status, genetic variation, postirradiation survival interval and comorbidities such as cancer, hypertension and diabetes mellitus (33–35). These factors can be controlled for in rodent studies, and radiation-induced changes in the brain have been extensively characterized in rodents, including impairments in neurogenesis (36–38), changes in dendritic spine morphology and density (39–41), changes in neuroinflammation and ATP production (18), impaired glutamatergic neurotransmission (42–46), and increased astrocytic and microglial inflammation (47–55). However, rodents do not develop white matter necrosis after fractionated whole-brain irradiation (fWBI) (44, 56–58), and differences in neuroanatomy [(e.g., greater hippocampal relative brain volume, larger gray:-white matter ratio) (59–61)] and limited inter-individual genetic variability (62) may limit

the translatability of findings. In contrast to rodents, non-human primates have greater neuroanatomic and genomic homology to humans and more fully recapitulate the histopathologic features of late-delayed radiation-induced brain injury (RIBI) after fWBI (e.g., cerebrovascular and white matter injury) (63–68).

The Radiation Countermeasures Center of Research Excellence (RadCCORE) non-human primate Radiation Survivor Cohort (RSC) is a unique resource in which rhesus macaques that have survived high-dose TBI (1.14–8.5 Gy) are adopted and monitored longitudinally for the development of late-delayed sequelae of radiation exposure. In this cohort, differences in diet and environment are controlled for, and health status extensively characterized (e.g., cardiac function, metabolic status, immune function, cancer surveillance), which makes this cohort ideal for the study of late effects of TBI and interactions between comorbid radiation-induced conditions.

Although the long-term consequences of single-high-dose TBI on the adult brain are unclear, fWBI for the treatment of brain cancer may result in neuroinflammation, white matter necrosis, vascular injury and cognitive impairment (69–72). In affected patients, scattered foci of hemorrhage and necrosis consistent with small blood vessel injury are detectable on susceptibility-weighted (SWI) magnetic resonance images (MRI) (73–78). In the current study, we hypothesized that non-human primate long-term survivors of high-dose TBI would develop lesions on imaging that were similar to those observed after fWBI, although less severe and with a longer latency period.

MATERIALS AND METHODS

Subjects

Magnetic resonance imaging (MRI) scans acquired between 2011 and 2018 were evaluated from 173 rhesus macaques, aged 2.8–18.3 years (median age: 6.5 years). Of these animals, 141 were males and 32 were females. In addition, 53 animals (50 males, 3 females; median age: 6.2 years, range: 3.5–18.3) had no prior history of irradiation and were either part of unrelated studies or adopted as control comparators and enrolled within the non-human primate Radiation Survivor Cohort (RSC). A total of 120 animals (91 males, 29 females; median age: 6.5 years, range: 2.8–16.5 years) were administered single-dose TBI (median dose: 6.6 Gy, range: 1.14–8.5 Gy) as part of separate studies at other institutions [Wake Forest University (Winston-Salem, NC); University of Maryland (College Park, MD), University of Illinois (Urbana-Champaign, IL); Armed Forces Radiobiology Research Institute (Bethesda, MD); Lovelace Respiratory Research Institute (Albuquerque, NM); and Citox Labs (Stillwell, KS)] and then adopted into the RSC for long-term surveillance for the sequelae of radiation exposure. Additional detail on irradiation methods, supportive care strategies, and acute effects for many animals donated to this cohort have been recently reported elsewhere (79–81), and are summarized in Supplementary Table S1 (https://doi.org/10.1667/RADE-20-00051.1.S1). Tabulated demographic data include age, radiation dose, dose rate and age at irradiation (Table 1).

Animals were housed in either stainless-steel cages in temperature- and humidity-controlled rooms with a 12:12 h light-dark schedule, or indoor-outdoor pens; animals were socially

housed whenever possible. Diet was contingent upon the experimental study in which the animal was enrolled; animals were either fed commercially available monkey chow (Purinat®, St. Louis, MO) or Typical American Primate diet (LabDiet 5L0P; Land O'Lakes Inc., St. Louis, MO] designed to approximate the macronutrients of a Western dietary profile. All animals received daily clinical assessment by trained veterinary personnel, including cage-side neurologic evaluation when indicated; all animals were neurologically normal. All procedures were approved by the Wake Forest University School of Medicine (WFUSM) Institutional Animal Care and Use Committee (IACUC) and performed in accordance with all state and federal animal welfare laws. WFUSM is accredited by the Association for Assessment and Accreditation of Laboratory Animal Care (AAALAC).

Magnetic Resonance Imaging

Animals were sedated with ketamine HCl (15 mg/kg body weight, IM) and maintained on inhaled isoflurane (3% induction, 1.5% maintenance) in 100% oxygen anesthesia for the duration of the MRI procedure. Images were acquired on a 3.0-Tesla Siemens Skyra clinical magnetic resonance scanner (Malvern, PA), operating on a D13 platform with a maximum gradient field strength = 45 mT/m. Sequences were optimized for non-human primates and acquired using a dedicated, 8 channel, non-human primate radiofrequency coil (Rapid MR International, Columbus, OH) tuned to 127.7 MHz.

T1-weighted anatomic images were obtained using a 3D volumetric magnetization-prepared rapid acquisition with gradient echo (MPRAGE) sequence (TR = 2,700 ms; TE = 3.39 ms; TI = 880 ms; FA=8 degrees; 160 slices, voxel dimension =0.5×0.5×0.5 mm^3). Brain lesions consistent with hemorrhage and necrosis were identified by susceptibility-weighted image (SWI) sequence (TR =28 ms, TE=20 ms, flip angle=15 degrees, NEX=2, with voxel size=0.5×0.5×0.5 mm^3). SWI and T1 sequences were co-registered, and the anatomic location of SWI-hypointense foci was determined from the corresponding T1 structural image. All lesion dimensions were calculated from T1 structural images. Lesion diameters were measured in three perpendicularly-oriented planes; volume was estimated assuming ellipsoid shape $\left(\frac{\pi}{6}abc\right)$, where a, b and c represent the axial, coronal and sagittal diameters.

Clinical Data

Archived data regarding comorbid conditions were retrieved from an internal animal medical records system and assessed for evidence of type II diabetes mellitus (T2DM) and hypertension. A diagnosis of T2DM was assigned by laboratory clinical veterinary personnel and was determined by clinical presentation including hyperglycemia, glucosuria or ketonuria, dyslipidemia, elevated hemoglobin A1C and/or glucose tolerance test results. Hypertension was defined as systolic blood pressure >30 mmHg and/or diastolic blood pressure >80 mmHg; the average of the three most recent measurements of systolic and diastolic blood pressure for each animal were used.

Statistical Analyses

All statistical analyses were completed using GraphPad Prism version 7.0 (La Jolla, CA). Animals were stratified by irradiation and SWI lesion status. Normality was assessed using

Shapiro-Wilk test. Non-parametric data (age at irradiation, age at lesion diagnosis, dose, dose rate, and irradiation-to-diagnosis interval) were compared by Mann Whitney U. The age at time of assessment between nonirradiated, irradiated NSL (no significant lesions) and irradiated SWI groups was compared using Kruskal-Wallis one-way analysis of variance (ANOVA). Outliers for lesion number were determined by ROUT method (Q = 1%; GraphPad Prism). The correlation between radiation dose (Gy) and lesion volume was assessed using two-tailed Spearman correlation.

The associations between prior radiation exposure and brain lesions on MRI, and between comorbid health conditions (T2DM and hypertension) and brain lesions on MRI were assessed using Fisher's exact test and the odds ratio calculated by Woolf logit method. Significance for all analyses was set to $P \leq 0.05$.

RESULTS

Susceptibility-Weighted Imaging (SWI) Hypointense Brain Lesions on MRI

Focal and multifocal T1-hypointense, SWI-hypointense brain lesions consistent with necrosis and/or cerebrovascular injury were noted in 13% of irradiated NHP and 0% of nonirradiated comparators (Fig. 1, Table 2). Prior TBI was associated with an increased risk of developing a lesion detectable by MRI (Fisher's exact, $P = 0.003$). No significant proprioceptive, locomotor or cranial nerve deficits were noted on cage-side neurologic evaluation.

Animals that developed brain lesions received higher doses of TBI (Fig. 2, Table 1) than animals that did not develop SWI-hypointense lesions; there was no statistically significant difference in dose rate. Twelve out of 16 (12/16) animals had at least one brain lesion present at the time of the first MRI evaluation; 7/16 animals developed nascent lesions during the study period (Fig. 3), of which 4/7 had no antecedent lesions. Nascent lesions (n = 11) developed 3.7–11.3 years postirradiation (median: 7.3 years) at 9.9–15.6 years of age (median: 11.3 years). There were no statistically significant differences in radiation dose or age at irradiation between animals that developed nascent lesions and those with antecedent lesions only.

There were 55 SWI-hypointense brain lesions across 16 animals; 14 out of 16 animals had 1–3 lesions and the remaining animals had 16 lesions each (n = 2) (Fig. 4A). No statistically significant relationship was found between radiation dose and SWI lesion number (Fig. 4B). Lesions occurred most frequently within the cerebrum (89%), with predilection for the occipital lobe (45%) (Table 3). Seventeen lesions were below the resolution capability of the T1-weighted sequence, precluding further neuroanatomic evaluation. Of the remaining lesions (38/55), the majority occurred within white matter or at the gray-white junction (50% and 29%, respectively); 21% occurred within gray matter. Lesions were equally distributed between hemispheres (right: n = 27; left: n = 28)

SWI and T1-weighted images were aligned, and lesion volumes calculated from the corresponding T1-weighted structural image to circumvent overestimation of lesion size due to the blooming artifact inherent in SWI (82). The majority of lesions (47/55, 85%) were

≤1.0 × 1.0 × 1.0 mm^3 (0.5 mm^3), 17 of which were below the resolution capacity of the T1-weighted sequence and recorded with a lesion volume of 0 mm^3. The median cumulative lesion volume per animal was 1.3 mm^3 (range: 0–14.9 mm^3). Longitudinal volumetric data were available for 26 lesions (n = 11 subjects); once present, the majority of lesions did not change in size over time (62%, 16/26 lesions), while 9 lesions increased in volume (n = 5 subjects). One lesion was no longer present on re-evaluation one year later. No statistically significant relationship was found between median or cumulative lesion volume and radiation dose (Gy) ($P > 0.05$).

Clinical Data

The associations between comorbid health conditions (T2DM and hypertension) and brain lesion presence were individually assessed. No statistically significant association between T2DM or hypertension and brain lesion status was detected.

Correlative Gross and Histopathology

Of the 16 animals diagnosed with SWI-hypointense brain lesions, two animals (Table 4) were humanely euthanized due to illnesses unassociated with neurologic dysfunction. NHP1 was euthanized due to the presence of multiple neoplasms (chondrolipoma, renal carcinoma, and poorly-differentiated neuroendocrine neoplasia) and poor prognosis. There was no gross or histologic evidence of metastatic disease. NHP2 was euthanized due to persistent bacterial pneumonia despite antibiotic treatment and supportive care, concurrent heart murmur, and T2DM.

In NHP1, a focal SWI hypointensity with corresponding 2.2 × 1.7 × 1.7 mm^3 (3.3 mm^3) T1 parenchymal defect was observed within the deep white matter of the caudal right occipital lobe at the time of first MRI assessment 5.8 years postirradiation (Fig. 5A and B). At reassessment 7.3 years postirradiation, the lesion had increased to 2.3 × 2.5 × 2.4 mm^3 (7.2 mm^3). At this time, a second SWI-hypointense focus with corresponding 5.9 × 1.2 × 0.9 mm^3 (3.3 mm^3) T1 parenchymal defect was found within the area between the right optic tract and globus pallidus. Gross evaluation of the occipital lobe revealed an irregular area of hemorrhage (Fig. 5C); histopathology revealed a focal vascular malformation resembling a cavernous hemangioma (Fig. 6A). There was scant hemorrhage in the ventral leptomeninges adjacent to the optic chiasm. An artery adjacent to the optic tract was segmentally, transmurally disrupted and replaced by aggregates of eosinophilic extracellular matrix and hemosiderin-laden macrophages (Fig. 6B). Distal segments were tortuous and redundant, with partial-to-complete occlusion of the vascular lumina by eosinophilic extracellular matrix and smooth muscle hyperplasia (Fig. 6C). White matter tracts adjacent to both vascular morphologic abnormalities were vacuolated, and there was axonal degeneration (swollen axons, dilated myelin sheathes and digestion chambers) within the cerebral peduncle.

In NHP2, no significant lesions were noted at the time of first MRI assessment 5.9 years postirradiation. At 6.8 years postirradiation, there was a focal SWI hypointensity with corresponding 0.4 × 0.3 × 0.3 mm^3 (0.02 mm^3) T1 parenchymal defect within the deep white matter of the left ventromedial occipital lobe. This lesion was present at reassessment

8.4 and 9.4 years postirradiation and did not change in size over time. The lesion could not be found grossly or histopathologically. A second SWI hypointensity with corresponding 0.4 × 0.4 × 0.4 mm^3 (0.03 mm^3) T1 parenchymal defect was noted within the white matter of the left prefrontal lobe at 8.4 and 9.4 years postirradiation. The lesion did not change in size over time. Grossly, there was focal hemorrhage within the prefrontal white matter. The corresponding histopathology evaluation revealed dilated tortuous vasculature with extensive perivascular extracellular matrix and chronic hemorrhage, morphologically consistent with radiation-induced cerebrovascular injury.

Cerebrovascular injury occurring without a premonitory SWI lesion was noted in one animal at the time of necropsy, after humane euthanasia necessitated by the occurrence of hepatocellular carcinoma (10.2 years of age, 5.4 years after 7.2 Gy TBI). On sectioned surface, there was regionally extensive congestion within the deep white matter of the right occipital lobe. Histopathology revealed a 4 × 5 mm^2 focus in which the deep white matter was infiltrated by irregularly dilated small- to medium-caliber blood vessels (telangiectasia, Fig. 6D). There were no SWI-hypointense lesions within the occipital lobe on a routine surveillance MRI conducted six months prior to necropsy.

DISCUSSION

Herein we have documented the prevalence of brain lesions consistent with focal or multifocal vascular injury in a cohort of rhesus macaque long-term survivors of single, high-dose TBI. We also provide two case reports detailing the corresponding histopathologic findings. These data add to a growing body of literature which suggests that the brain is vulnerable to radiation injury at doses lower than the CNS-ARS threshold.

Magnetic resonance imaging is a non-invasive imaging technique used to evaluate the response of hydrogen atoms to magnetic fields and radiofrequency pulses to reconstruct structural and functional tissue parameters as visual data. Modulation of the applied radiofrequency pulses in specific “sequences” is used to assess different biological tissue characteristics. In the current study, T1-weighted MPRAGE sequences were used to acquire anatomic brain images and provide contrast between gray and white matter. SWI is extremely sensitive to the presence of diamagnetic (calcium) and paramagnetic (iron, hemosiderin) substances within the body (82, 83), which appear as foci of “blooming” susceptibility/hypointense artifact. Thus these sequences can be used to identify hemorrhage and necrosis with mineralization in affected subjects. The SWI sequence is routinely used in clinical practice to identify blood products and small-volume microhemorrhages in human patients, and SWI hypointensities have been reported in cancer patients receiving brain radiotherapy (73, 74, 77, 78, 84–88). Use of these non-invasive, *in vivo* imaging protocols allows for monitoring of the progression of brain pathology longitudinally, often years prior to death, and offers the potential to map MRI abnormalities to neurologic deficits.

As animals in this study are currently enrolled in a cohort undergoing long-term surveillance for health effects of prior radiation exposure, animals are not euthanized until declining health status necessitates humane euthanasia. Therefore, our analyses were primarily limited to the evaluation of findings on magnetic resonance images acquired *in vivo*.

Histopathologic evaluation was limited to the two deceased animals noted to have SWI-hypointense lesions on MRI (14/16 are living). While caution should be used in extrapolating these results to the general population, the histopathologic appearance agrees with the imaging characteristics (73–75, 89, 90). Vascular malformations (cavernous hemangiomas) occur as a sequela of cerebral irradiation in humans (89, 91, 92). Despite previous categorization as “hemangiomas,” these focal structural abnormalities are not presumed due to proliferation of endothelium, and in keeping with the International Society for the Study of Vascular Anomalies (ISSVA) classification system, are more correctly classified as “vascular malformations” (93). The remaining cerebrovascular lesions observed in this study (perivascular extracellular matrix with acute and chronic hemorrhage) are similar to lesions observed in late-delayed RIBI after fWBI in non-human primates and humans (64, 67, 68, 70, 90, 94, 95). These cases suggest the etiopathogenesis of late-delayed RIBI involves vascular injury characterized by inappropriate remodeling and resultant structural abnormalities. Identification of cerebrovascular injury at necropsy in the absence of a corresponding lesion on brain imaging, as had occurred in one animal, suggests that some of these lesions may develop rapidly. Additional studies will follow, including comprehensive histopathologic evaluation of the remaining 14/16 animals.

In one case, a lesion noted on MRI could not be located on gross or histopathologic evaluation, despite use of the MRI data during the trimming process and stereological sectioning. The identification of brain lesions at the time of prosection is limited by small lesion size, the relatively large volume of the non-human primate brain, and low optical contrast between foci of necrosis and normal tissue.

Our study was limited to the evaluation of postirradiation MRI, as animals within the cohort are adopted from separate studies in which acquisition of preirradiation brain MRI was not a part of the experimental design. Hemorrhages develop in the brain parenchyma and subarachnoid spaces in mice within 30 days after $LD_{50/30}$ TBI (9.5 Gy ^{60}Co), and occur in association with thrombocytopenia (17, 18, 96). Concurrent neuroinflammation, increased cytokine production and deficits in ATP biogenesis (18) may also predispose the cerebral vasculature to increased permeability or vascular necrosis, leading to parenchymal hemorrhage during the acute phases of radiation injury. Consequently, congenital lesions and residual iron resultant from thrombocytopenia or endothelial injury during ARS cannot be excluded as the cause of the lesions present at the time of first MRI assessment; however, the development of additional lesions during the study period in seven animals (3.7–11.3 years postirradiation) suggests a component of ongoing (chronic) cerebrovascular injury. The affected animals in the current study were not thrombocytopenic at the time of MRI. The absence of similar foci on MRI in nonirradiated controls supports the hypothesis that these lesions are radiation-induced. While cognitive assessment within this cohort has been limited due to subject unwillingness to engage with the task, preliminary analyses suggest that some animals may have reduced cognitive flexibility (97). Radiation-induced temporal microbleeds in cancer patients are independently associated with likelihood of cognitive dysfunction (78). SWI lesions in this cohort occur in the absence of neurological signs detectable by cranial nerve and proprioception testing. Further research evaluating the physiological and cognitive ramifications, and progression of these lesions, is needed and will be the focus of additional studies.

T2DM and cardiovascular disease are late-delayed effects of TBI and have been observed in this cohort of macaques (98, 99). As these conditions also have effects on the cerebral vasculature in the absence of radiation exposure, we evaluated the association between comorbid T2DM and hypertension on SWI lesion occurrence. No statistically significant association between concurrent T2DM or hypertension and SWI-hypointense brain lesions was found.

In summary, we have characterized the imaging prevalence of brain lesions compatible with cerebrovascular injury in a cohort of rhesus macaque long-term survivors of high dose TBI. We have determined that prior radiation exposure is associated with the development of SWI-hypointense brain lesions and provide evidence that the brain may be susceptible to injury at lower doses of radiation than those required to induce the ARS of the central nervous system (20–50 Gy) (3). These data suggest that human populations exposed to high-dose TBI may benefit from long-term follow-up including MRI to assess cerebrovascular injury.

Supplementary Material

Refer to Web version on PubMed Central for supplementary material.

ACKNOWLEDGMENTS

We acknowledge the efforts of the Cline Laboratory technical staff for their assistance in acquiring MRI images and providing care to animals within the RadCCORE RSC. This work was supported by NIH grant no. U19-AI67798 awarded to Nelson Chao, Duke University (JMC: primate core leader, Wake Forest School of Medicine). EGB was supported by NIH grant no. T35 OD 10946.

REFERENCES

1. Institute of Medicine (US) Committee on Medical Preparedness for a Terrorist Nuclear Event. Assessing medical preparedness to respond to a terrorist nuclear event: Workshop report. Benjamin GC, McGeary M, McCutchen SR, editors. Washington, DC: National Academies Press; 2009.
2. Fliedner TM, Dorr HD, Meineke V. Multi-organ involvement as a pathogenetic principle of the radiation syndromes: a study involving 110 case histories documented in SEARCH and classified as the bases of haematopoietic indicators of effect. Br J Radiol 2005; S27:1–8.
3. Acute radiation syndrome: A brochure for physicians. Atlanta, GA: Centers for Disease Control and Prevention; 2017.
4. Loganovsky K Do low doses of ionizing radiation affect the human brain? Data Sci J 2009; 8:PBR13–BR35.
5. Danilov VM, Pozdeev VK. The epileptiform reactions of the human brain to prolonged exposure to low-dose ionizing radiation. (Article in Russian). Fiziol Zh Im I M Sechenova 1994; 80:88–98.
6. Zhavoronkova LA, Kholodova NB, Zubovskii GA, Smirnov Yu N, Koptelov Yu M, Ryzhov NI. Electroencephalographic correlates of neurological disturbances at remote periods of the effect of ionizing radiation (sequelae of the Chernobyl' NPP accident). Neurosci Behav Physiol 1995; 25:142–9. [PubMed: 7630498]
7. Zhavoronkova LA, Kholodova NB, Zubovsky GA, Gogitidze NV, Koptelov YM. EEG power mapping, dipole source and coherence analysis in Chernobyl patients. Brain Topogr 1995; 8:161–8. [PubMed: 8793126]
8. Novikov VS, Tsygan VN, Borisova ED, Rybina LA. Changes in brain bioelectric activity in liquidators of sequelae of the accident at Chernobyl power plant. Fiziol Cheloveka 1997; 23:34–9. (Article in Russian)

9. Vyatleva OA, Katargina TA, Puchinskaya LM, Yurkin MM. Electrophysiological characterization of the functional state of the brain in mental disturbances in workers involved in the clean-up following the Chernobyl atomic energy station accident. Neurosci Behav Physiol 1997; 27:166–72. [PubMed: 9168487]
10. Zhavoronkova LA, Kholodova NB, Belostocky AP, Koulikov MA. Reduced electroencephalographic coherence asymmetry in the Chernobyl accident survivors. Span J Psychol 2008; 11:363–73. [PubMed: 18988424]
11. Zhavoronkova LA, Gogitidze NV, Kholodova NB. Postradiation changes in the brain asymmetry and higher mental functions of right- and left-handed subjects (the sequelae of the accident at the Chernobyl Atomic Electric Power Station). Zh Vyssh Nerv Deiat Im I P Pavlova 2000; 50:68–79. (Article in Russian) [PubMed: 10750190]
12. Ivanov VK, Maksioutov MA, Chekin SY, Petrov AV, Biryukov AP, Kruglova ZG, et al. The risk of radiation-induced cerebrovascular disease in Chernobyl emergency workers. Health Phys 2006; 90:199–207. [PubMed: 16505616]
13. Shimizu Y, Kodama K, Nishi N, Kasagi F, Suyama A, Soda M, et al. Radiation exposure and circulatory disease risk: Hiroshima and Nagasaki atomic bomb survivor data, 1950–2003. BMJ 2010; 340:b5349. [PubMed: 20075151]
14. Shimizu Y, Pierce DA, Preston DL, Mabuchi K. Studies of the mortality of atomic bomb survivors. Report 12, part II. Noncancer mortality: 1950–1990. Radiat Res 1999; 152:374–89. [PubMed: 10477914]
15. Preston DL, Shimizu Y, Pierce DA, Suyama A, Mabuchi K. Studies of mortality of atomic bomb survivors. Report 13: Solid cancer and noncancer disease mortality: 1950–1997. Radiat Res 2003; 160:381–407. [PubMed: 12968934]
16. Kharchenko VP, Zubovskii GA, Kholodova NB. Changes in the brain of persons who participated in the cleaning-up of the Chernobyl AES accident based on the data of radiodiagnosis (single-photon emission-computed radionuclide tomography, X-ray computed tomography and magnetic resonance tomography) (Article in Russian). Vestn Rentgenol Radiol 1995:11–4. [PubMed: 7653045]
17. Gorbunov NV, Kiang JG. Ghrelin therapy decreases incidents of intracranial hemorrhage in mice after whole-body ionizing irradiation combined with burn trauma. Int J Mol Sci 2017; 18:1693.
18. Kiang JG, Smith JT, Anderson MN, Umali MV, Ho C, Zhai M, et al. A novel therapy, using Ghrelin with pegylated G-CSF, inhibits brain hemorrhage from ionizing radiation or combined radiation injury. Pharm Pharmacol Int J 2019; 7:133–45.
19. Otake M, Schull WJ, Lee S. Threshold for radiation-related severe mental retardation in prenatally exposed A-bomb survivors: A reanalysis. Int J Radiat Biol 1996; 70:755–63. [PubMed: 8980673]
20. Otake M, Schull WJ. In utero exposure to A-bomb radiation and mental retardation; a reassessment. Br J Radiol 1984; 57:409–14. [PubMed: 6539140]
21. Otake M, Schull WJ. Radiation-related brain damage and growth retardation among the prenatally exposed atomic bomb survivors. Int J Radiat Biol 1998; 74:159–71. [PubMed: 9712546]
22. Schull WJ. Brain damage among individuals exposed prenatally to ionizing radiation: a 1993 review. Stem Cells 1997; 15:S129–33.
23. Valentin J Biological effects after prenatal irradiation (embryo and fetus): ICRP Publication 90 Approved by the Commission in October 2002. Ann ICRP 2003; 33:1–206.
24. Wood JW, Johnson KG, Omori Y, Kawamoto S, Keehn RJ. Mental retardation in children exposed in utero to the atomic bombs in Hiroshima and Nagasaki. Am J Public Health Nations Health 1967; 57:1381–9. [PubMed: 6069014]
25. Syrjala KL, Dikmen S, Langer SL, Roth-Roemer S, Abrams JR. Neuropsychologic changes from before transplantation to 1 year in patients receiving myeloablative allogeneic hematopoietic cell transplant. Blood 2004; 104:3386. [PubMed: 15251983]
26. Willard VW, Leung W, Huang Q, Zhang H, Phipps S. Cognitive outcome after pediatric stem-cell transplantation: impact of age and total-body irradiation. J Clin Oncol 2014; 32:3982–8. [PubMed: 25385724]

27. Shah AJ, Epport K, Azen C, Killen R, Wilson K, De Clerck D, et al. Progressive declines in neurocognitive function among survivors of hematopoietic stem cell transplantation for pediatric hematologic malignancies. J Pediatr Hematol Oncol 2008; 30:411–8. [PubMed: 18525456]
28. Simms S, Kazak AE, Golomb V, Goldwein J, Bunin N. Cognitive, behavioral, and social outcome in survivors of childhood stem cell transplantation. J Pediatr Hematol Oncol 2002; 24:115–9. [PubMed: 11990696]
29. Barrera M, Atenafu E. Cognitive, educational, psychosocial adjustment and quality of life of children who survive hematopoietic SCT and their siblings. Bone Marrow Transplant 2008; 42:15–21. [PubMed: 18372909]
30. Kramer JH, Crittenden MR, DeSantes K, Cowan MJ. Cognitive and adaptive behavior 1 and 3 years following bone marrow transplantation. Bone Marrow Transplant 1997; 19:607–13. [PubMed: 9085740]
31. Smedler AC, Bolme P. Neuropsychological deficits in very young bone marrow transplant recipients. Acta Paediatr 1995; 84:429–33. [PubMed: 7540899]
32. Perkins JL, Kunin-Batson AS, Youngren NM, Ness KK, Ulrich KJ, Hansen MJ, et al. Long-term follow-up of children who underwent hematopoeitic cell transplant (HCT) for AML or ALL at less than 3 years of age. Pediatr Blood Cancer 2007; 49:958–63. [PubMed: 17474113]
33. Hopewell JW, Wright EA. The nature of latent cerebral irradiation damage and its modification by hypertension. Br J Radiol 1970; 43:161–7. [PubMed: 5435118]
34. Kooistra M, Geerlings MI, Mali WP, Vincken KL, van der Graaf Y, Biessels GJ, et al. Diabetes mellitus and progression of vascular brain lesions and brain atrophy in patients with symptomatic atherosclerotic disease. The SMART-MR study. J Neurol Sci 2013; 332:69–74. [PubMed: 23835088]
35. Alsbeih G, El-Sebaie M, Al-Rajhi N, Al-Harbi N, Al-Hadyan K, Al-Qahtani S, et al. Among 45 variants in 11 genes, HDM2 promoter polymorphisms emerge as new candidate biomarker associated with radiation toxicity. 3 Biotech 2014; 4:137–48.
36. Bellinzona M, Gobbel GT, Shinohara C, Fike JR. Apoptosis is induced in the subependyma of young adult rats by ionizing irradiation. Neurosci Lett 1996; 208:163–6. [PubMed: 8733295]
37. Mizumatsu S, Monje ML, Morhardt DR, Rola R, Palmer TD, Fike JR. Extreme sensitivity of adult neurogenesis to low doses of X-irradiation. Cancer Res 2003; 63:4021–7. [PubMed: 12874001]
38. Monje ML, Mizumatsu S, Fike JR, Palmer TD. Irradiation induces neural precursor-cell dysfunction. Nat Med 2002; 8:955–62. [PubMed: 12161748]
39. Ji S Cranial irradiation altered dendritic spine complexity in the rat hippocampus and induced memory decline. Int J Radiat Oncol Biol Phys 99:E599.
40. Chakraborti A, Allen A, Allen B, Rosi S, Fike JR. Cranial irradiation alters dendritic spine density and morphology in the hippocampus. PloS One 2012; 7:e40844. [PubMed: 22815839]
41. Parihar VK, Limoli CL. Cranial irradiation compromises neuronal architecture in the hippocampus. Proc Natl Acad Sci U S A 2013; 110:12822–7. [PubMed: 23858442]
42. Machida M, Lonart G, Britten RA. Low (60 cGy) doses of (56)Fe HZE-particle radiation lead to a persistent reduction in the glutamatergic readily releasable pool in rat hippocampal synaptosomes. Radiat Res 2010; 174:618–23. [PubMed: 20726706]
43. Rohde BH, Rea MA, Simon JR, McBride WJ. Effects of X-irradiation induced loss of cerebellar granule cells on the synaptosomal levels and the high affinity uptake of amino acids. J Neurochem 1979; 32:1431–5. [PubMed: 35587]
44. Shi L, Adams MM, Long A, Carter CC, Bennett C, Sonntag WE, et al. Spatial learning and memory deficits after whole-brain irradiation are associated with changes in NMDA receptor subunits in the hippocampus. Radiat Res 2006; 166:892–9. [PubMed: 17149974]
45. Wu PH, Coultrap S, Pinnix C, Davies KD, Tailor R, Ang KK, et al. Radiation induces acute alterations in neuronal function. PloS One 2012; 7:e37677. [PubMed: 22662188]
46. Moore ED, Kooshki M, Wheeler KT, Metheny-Barlow LJ, Robbins ME. Differential expression of Homer1a in the hippocampus and cortex likely plays a role in radiation-induced brain injury. Radiat Res 2014; 181:21–32. [PubMed: 24377717]

47. Moore ED, Kooshki M, Metheny-Barlow LJ, Gallagher PE, Robbins ME. Angiotensin-(1–7) prevents radiation-induced inflammation in rat primary astrocytes through regulation of MAP kinase signaling. Free Radic Biol Med 2013; 65:1060–8. [PubMed: 24012919]
48. Kyrkanides S, Moore AH, Olschowka JA, Daeschner JC, Williams JP, Hansen JT, et al. Cyclooxygenase-2 modulates brain inflammation-related gene expression in central nervous system radiation injury. Brain Res Mol Brain Res 2002; 104:159–69. [PubMed: 12225870]
49. Kyrkanides S, Olschowka JA, Williams JP, Hansen JT, O'Banion MK. TNF alpha and IL-1beta mediate intercellular adhesion molecule-1 induction via microglia-astrocyte interaction in CNS radiation injury. J Neuroimmunol 1999; 95:95–106. [PubMed: 10229119]
50. Olschowka JA, Kyrkanides S, Harvey BK, O'Banion MK, Williams JP, Rubin P, et al. ICAM-1 induction in the mouse CNS following irradiation. Brain Behav Immun 1997; 11:273–85. [PubMed: 9512815]
51. Chiang CS, McBride WH, Withers HR. Radiation-induced astrocytic and microglial responses in mouse brain. Radiother Oncol 1993; 29:60–8. [PubMed: 8295989]
52. Schnegg CI, Kooshki M, Hsu FC, Sui G, Robbins ME. PPARdelta prevents radiation-induced proinflammatory responses in microglia via transrepression of NF-kappaB and inhibition of the PKCalpha/MEK1/2/ERK1/2/AP-1 pathway. Free Radic Biol Med 2012; 52:1734–43. [PubMed: 22387176]
53. Hwang SY, Jung JS, Kim TH, Lim SJ, Oh ES, Kim JY, et al. Ionizing radiation induces astrocyte gliosis through microglia activation. Neurobiol Dis 2006; 21:457–67. [PubMed: 16202616]
54. Zhou K, Bostrom M, Ek CJ, Li T, Xie C, Xu Y, et al. Radiation induces progenitor cell death, microglia activation, and blood-brain barrier damage in the juvenile rat cerebellum. Sci Rep 2017; 7:46181. [PubMed: 28382975]
55. Ramanan S, Kooshki M, Zhao W, Hsu F-C, Robbins ME. PPAR-alpha ligands inhibit radiation-induced microglial inflammatory responses by negatively regulating NF-kappaB and AP-1 pathways. Free Radic Biol Med 2008; 45:1695–704. [PubMed: 18852043]
56. Brown WR, Thore CR, Moody DM, Robbins ME, Wheeler KT. Vascular damage after fractionated whole-brain irradiation in rats. Radiat Res 2005; 164:662–8. [PubMed: 16238444]
57. Shi L, Linville MC, Iversen E, Molina DP, Yester J, Wheeler KT, et al. Maintenance of white matter integrity in a rat model of radiation-induced cognitive impairment. J Neurol Sci 2009; 285:178–84. [PubMed: 19625028]
58. Robbins ME, Payne V, Tommasi E, Diz DI, Hsu FC, Brown WR, et al. The AT1 receptor antagonist, L-158,809, prevents or ameliorates fractionated whole-brain irradiation-induced cognitive impairment. Int J Radiat Oncol Biol Phys 2009; 73:499–505. [PubMed: 19084353]
59. Zhang K, Sejnowski TJ. A universal scaling law between gray matter and white matter of cerebral cortex. Proc Natl Acad Sci U S A 2000; 97:5621–6. [PubMed: 10792049]
60. Badea A, Ali-Sharief AA, Johnson GA. Morphometric analysis of the C57BL/6J mouse brain. Neuroimage 2007; 37:683–93. [PubMed: 17627846]
61. Shamy JL, Buonocore MH, Makaron LM, Amaral DG, Barnes CA, Rapp PR. Hippocampal volume is preserved and fails to predict recognition memory impairment in aged rhesus monkeys (Macaca mulatta). Neurobiol Aging 2006; 27:1405–15. [PubMed: 16183171]
62. Rivera J, Tessarollo L. Genetic background and the dilemma of translating mouse studies to humans. Immunity 2008; 28:1–4. [PubMed: 18199409]
63. Caveness WF. Pathology of radiation damage to the normal brain of the monkey. Natl Cancer Inst Monogr 1977; 46:57–76. [PubMed: 418344]
64. Hanbury DB, Robbins ME, Bourland JD, Wheeler KT, Peiffer AM, Mitchell EL, et al. Pathology of fractionated whole-brain irradiation in rhesus monkeys (Macaca mulatta). Radiat Res 2015; 183:367–74. [PubMed: 25688996]
65. Nakagaki H, Brunhart G, Kemper TL, Caveness WF. Monkey brain damage from radiation in the therapeutic range. J Neurosurg 1976; 44:3–11. [PubMed: 811769]
66. Wakisaka S, O'Neill RR, Kemper TL, Verrelli DM, Caveness WF. Delayed brain damage in adult monkeys from radiation in the therapeutic range. Radiat Res 1979; 80:277–91. [PubMed: 116311]
67. Andrews RN, Caudell DL, Metheny-Barlow LJ, Peiffer AM, Tooze JA, Bourland JD, et al. Fibronectin produced by cerebral endothelial and vascular smooth muscle cells contributes to

perivascular extracellular matrix in late-delayed radiation-induced brain injury. Radiat Res 2018; 190:361–73. [PubMed: 30016219]

68. Andrews RN, Metheny-Barlow LJ, Peiffer AM, Hanbury DB, Tooze JA, Bourland JD, et al. Cerebrovascular remodeling and neuroinflammation is a late effect of radiation-induced brain injury in non-human primates. Radiat Res 2017; 187:599–611. [PubMed: 28398880]
69. DeAngelis LM, Delattre JY, Posner JB. Radiation-induced dementia in patients cured of brain metastases. Neurology 1989; 39:789–96. [PubMed: 2725874]
70. Di Chiro G, Oldfield E, Wright DC, De Michele D, Katz DA, Patronas NJ, et al. Cerebral necrosis after radiotherapy and/or intraarterial chemotherapy for brain tumors: PET and neuropathologic studies. AJR Am J Roentgenol 1988; 150:189–97. [PubMed: 3257119]
71. Crossen JR, Garwood D, Glatstein E, Neuwelt EA. Neurobehavioral sequelae of cranial irradiation in adults: a review of radiation-induced encephalopathy. J Clin Oncol 1994; 12:627–42. [PubMed: 8120563]
72. Vigliani MC, Duyckaerts C, Hauw JJ, Poisson M, Magdelenat H, Delattre JY. Dementia following treatment of brain tumors with radiotherapy administered alone or in combination with nitrosourea-based chemotherapy: a clinical and pathological study. J Neurooncol 1999; 41:137–49. [PubMed: 10222434]
73. Morrison MA, Hess CP, Clarke JL, Butowski N, Chang SM, Molinaro AM, et al. Risk factors of radiotherapy-induced cerebral microbleeds and serial analysis of their size compared with white matter changes: A 7T MRI study in 113 adult patients with brain tumors. J Magn Reson Imaging 2019; 50:868–77. [PubMed: 30663150]
74. Varon D, Simons M, Chiang F, Tedesqui G, Pacheco G, Martinez P, et al. Brain radiation-related black dots on susceptibility-weighted imaging. Neuroradiol J 2014; 27:445–51. [PubMed: 25196618]
75. Tanino T, Kanasaki Y, Tahara T, Michimoto K, Kodani K, Kakite S, et al. Radiation-induced microbleeds after cranial irradiation: evaluation by phase-sensitive magnetic resonance imaging with 3.0 tesla. Yonago Acta Med 2013; 56:7–12. [PubMed: 24031146]
76. Bian W, Hess CP, Chang SM, Nelson SJ, Lupo JM. Susceptibility-weighted MR imaging of radiation therapy-induced cerebral microbleeds in patients with glioma: a comparison between 3T and 7T. Neuroradiology 2014; 56:91–6. [PubMed: 24281386]
77. Wahl M, Anwar M, Hess CP, Chang SM, Lupo JM. Relationship between radiation dose and microbleed formation in patients with malignant glioma. Radiat Oncol 2017; 12:126. [PubMed: 28797254]
78. Shen Q, Lin F, Rong X, Yang W, Li Y, Cai Z, et al. Temporal cerebral microbleeds are associated with radiation necrosis and cognitive dysfunction in patients treated for nasopharyngeal carcinoma. Int J Radiat Oncol Biol Phys 2016; 94:1113–20. [PubMed: 27026315]
79. Farese AM, Cohen MV, Katz BP, Smith CP, Jackson W 3rd, Cohen DM, et al. A nonhuman primate model of the hematopoietic acute radiation syndrome plus medical management. Health Phys 2012; 103:367–82. [PubMed: 22929469]
80. MacVittie TJ, Farese AM, Jackson W 3rd. The hematopoietic syndrome of the acute radiation syndrome in rhesus macaques: A systematic review of the lethal dose response relationship. Health Phys 2015; 109:342–66. [PubMed: 26425897]
81. Yu JZ, Lindeblad M, Lyubimov A, Neri F, Smith B, Szilagyi E, et al. Subject-based versus population-based care after radiation exposure. Radiat Res 2015; 184:46–55. [PubMed: 26121229]
82. Schenck JF. The role of magnetic susceptibility in magnetic resonance imaging: MRI magnetic compatibility of the first and second kinds. Med Phys 1996; 23:815–50. [PubMed: 8798169]
83. Schweser F, Deistung A, Lehr BW, Reichenbach JR. Differentiation between diamagnetic and paramagnetic cerebral lesions based on magnetic susceptibility mapping. Med Phys 2010; 37:5165–78. [PubMed: 21089750]
84. Bian W, Hess CP, Chang SM, Nelson SJ, Lupo JM. Computer-aided detection of radiation-induced cerebral microbleeds on susceptibility-weighted MR images. Neuroimage Clin 2013; 2:282–90. [PubMed: 24179783]

85. Lupo JM, Chuang CF, Chang SM, Barani IJ, Jimenez B, Hess CP, et al. 7-Tesla susceptibility-weighted imaging to assess the effects of radiotherapy on normal-appearing brain in patients with glioma. Int J Radiat Oncol Biol Phys 2012; 82:e493–e500. [PubMed: 22000750]

86. Roongpiboonsopit D, Kuijf HJ, Charidimou A, Xiong L, Vashkevich A, Martinez-Ramirez S, et al. Evolution of cerebral microbleeds after cranial irradiation in medulloblastoma patients. Neurology 2017; 88:789–96. [PubMed: 28122904]

87. Belliveau JG, Bauman GS, Tay KY, Ho D, Menon RS. Initial investigation into microbleeds and white matter signal changes following radiotherapy for low-grade and benign brain tumors using ultra-high-field MRI techniques. AJNR Am J Neuroradiol 2017; 38:2251–6. [PubMed: 28970242]

88. Phillips NS, Hillenbrand CM, Mitrea BG, Yan J, Li C, Scoggins MA, et al. Cerebral microbleeds in adult survivors of childhood acute lymphoblastic leukemia treated with cranial radiation. Sci Rep 2020; 10:692.

89. Cutsforth-Gregory JK, Lanzino G, Link MJ, Brown RD Jr., Flemming KD. Characterization of radiation-induced cavernous malformations and comparison with a nonradiation cavernous malformation cohort. J Neurosurg 2015; 122:1214–22. [PubMed: 25699412]

90. Guez D, Last D, Daniels D, Sharabi S, Nass D, Nissim O, et al. Radiation-induced vascular malformations in the brain, mimicking tumor in MRI-based treatment response assessment maps (TRAMs). Clin Transl Radiat Oncol. 2018; 15:1–6. [PubMed: 30547098]

91. Jain R, Robertson PL, Gandhi D, Gujar SK, Muraszko KM, Gebarski S. Radiation-induced cavernomas of the brain. AJNR Am J Neuroradiol 2005; 26:1158–62. [PubMed: 15891176]

92. Heckl S, Aschoff A, Kunze S. Radiation-induced cavernous hemangiomas of the brain: a late effect predominantly in children. Cancer 2002; 94:3285–91. [PubMed: 12115362]

93. Steele L, Zbeidy S, Thomson J, Flohr C. How is the term haemangioma used in the literature? An evaluation against the revised ISSVA classification. Pediatr Dermatol 2019; 36:628–33. [PubMed: 31318089]

94. Martins AN, Johnston JS, Henry JM, Stoffel TJ, Di Chiro G. Delayed radiation necrosis of the brain. J Neurosurg 1977; 47:336–45. [PubMed: 894340]

95. Valk PE, Dillon WP. Radiation injury of the brain. AJNR Am J Neuroradiol 1991; 12:45–62. [PubMed: 7502957]

96. Wong K, Chang PY, Fielden M, Downey AM, Bunin D, Bakke J, et al. Pharmacodynamics of romiplostim alone and in combination with pegfilgrastim on acute radiation-induced thrombocytopenia and neutropenia in non-human primates. Int J Radiat Biol 2020; 96:155–66. [PubMed: 31216213]

97. Hanbury DB, Peiffer AM, Dugan G, Andrews RN, Cline JM. Long-term cognitive functioning in single-dose total-body gamma-irradiated rhesus monkeys (Macaca mulatta). Radiat Res 2016; 186:447–54. [PubMed: 27740889]

98. Kavanagh K, Dendinger MD, Davis AT, Register TC, DeBo R, Dugan G, et al. Type 2 diabetes is a delayed late effect of whole-body irradiation in nonhuman primates. Radiat Res 2015; 183:398–406. [PubMed: 25811716]

99. DeBo RJ, Lees CJ, Dugan GO, Caudell DL, Michalson KT, Hanbury DB, et al. Late effects of total-body gamma irradiation on cardiac structure and function in male rhesus macaques. Radiat Res 2016; 186:55–64. [PubMed: 27333082]

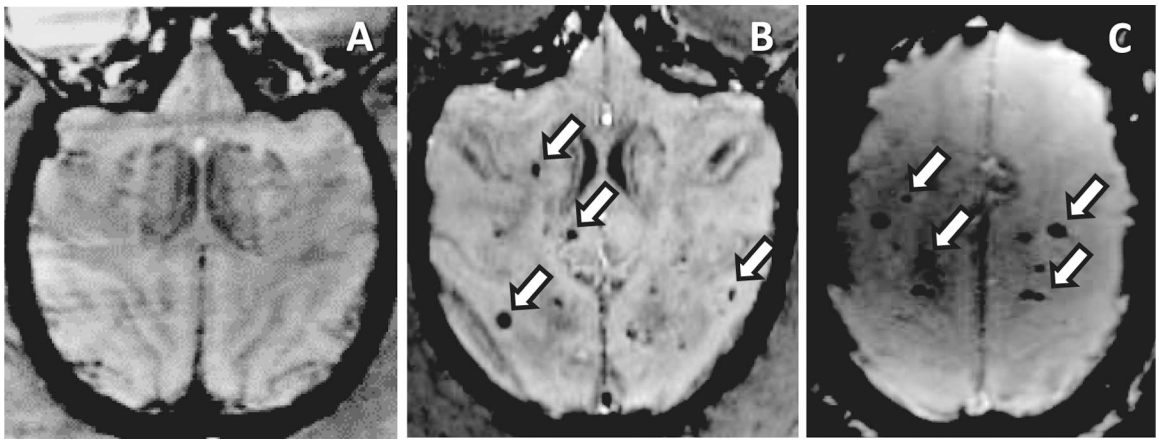

FIG. 1.

Animals receiving TBI develop hypointense lesions on susceptibility-weighted imaging (SWI-MRI) comparable to those which occur in RIBI after fWBI. Panel A: There are no SWI-hypointense foci in nonirradiated animals. Panel B: Multifocal SWI-hypointense foci (white arrows) are scattered throughout the cerebrum of an animal that developed RIBI after receiving 40 Gy fWBI (8 × 5 Gy fractions, 2× per week) as part of a separate study. Scan taken at 12 months postirradiation. Panel C: Comparable, multifocal SWI-hypointense foci in a long-term TBI survivor; the subject received 8.0 Gy TBI one year prior to MRI. White arrows indicate foci of hemorrhage and/or necrosis.

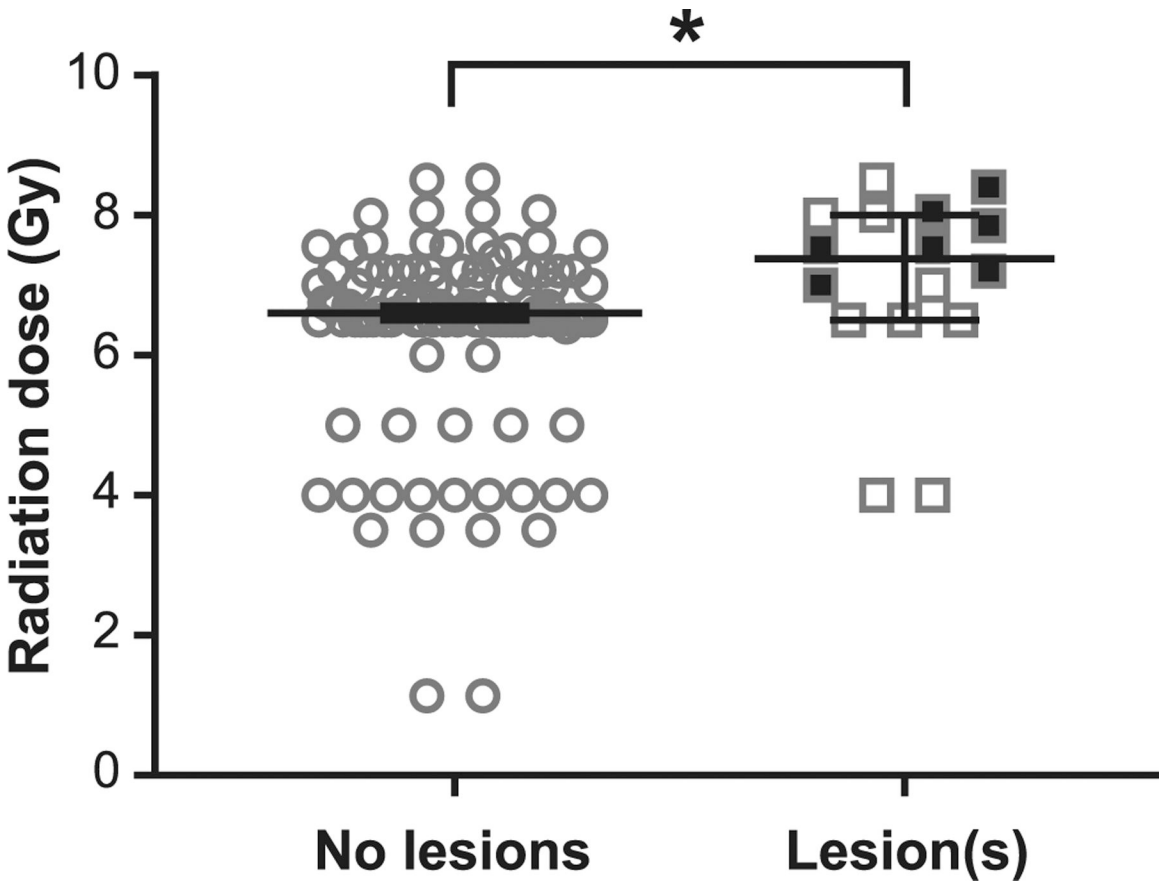

FIG. 2.

TBI is associated with MRI-detectable brain lesions, which occur at higher doses. Animals that developed brain lesions after TBI received higher doses than those without lesions (median: 7.4 Gy vs. 6.6 Gy, respectively; $P < 0.02$). Filled squares indicate incident lesions which occurred during the surveillance period; these animals received higher doses during TBI (7.8 Gy ± 0.4 SD) than those with lesions present since the time of first evaluation only (6.6 ± 1.5 SD) ($P < 0.05$). Bars indicate median value, error bars are 95% confidence interval. *$P < 0.05$.

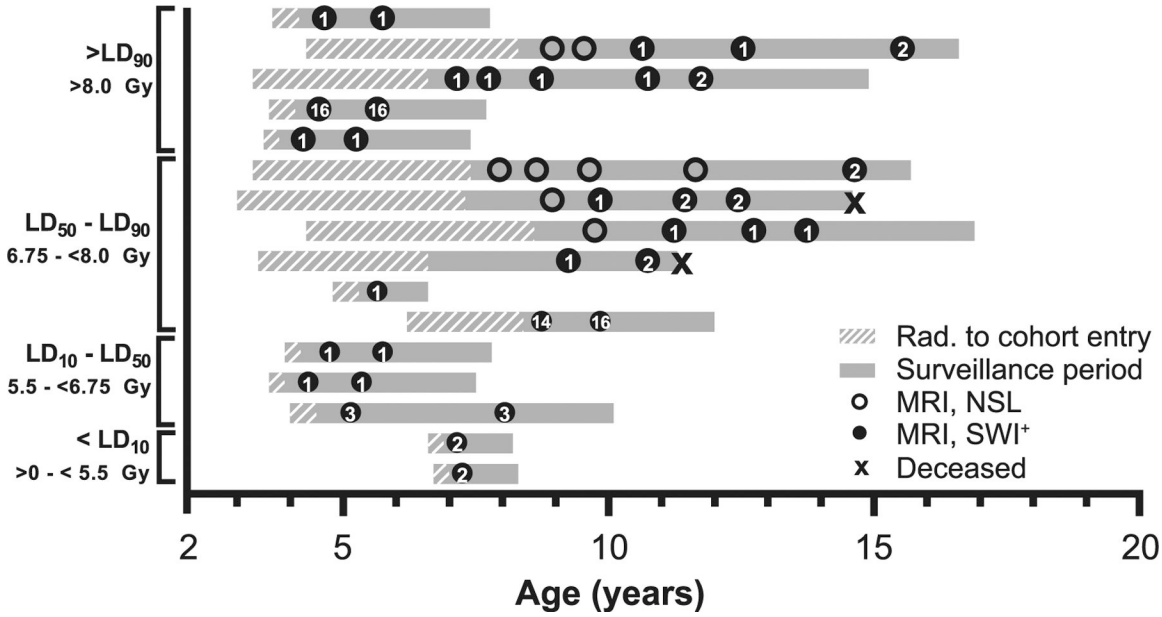

FIG. 3.

Radiologic and life history of animals with SWI-hypointense foci. Each gray bar represents a single animal; animals are listed in order of decreasing radiation dose. Bars begin at age at irradiation; cross-hatched region indicates the period before adoption and cohort enrollment. The solid gray region indicates the period the animal was enrolled within the Radiation Survivors Cohort. Circles indicate brain MRI examinations; open circles represent MRI with no significant lesions (NSL), closed circles represent a SWI lesion that was present. Arabic numerals within closed circles indicate the number of SWI foci at the time of examination. "X" indicates the age at death of deceased animals (n = 2). Lethal dose (LD) stratifications refer to LD_{30} for the hematopoietic acute radiation syndrome (H-ARS) in rhesus macaques (80).

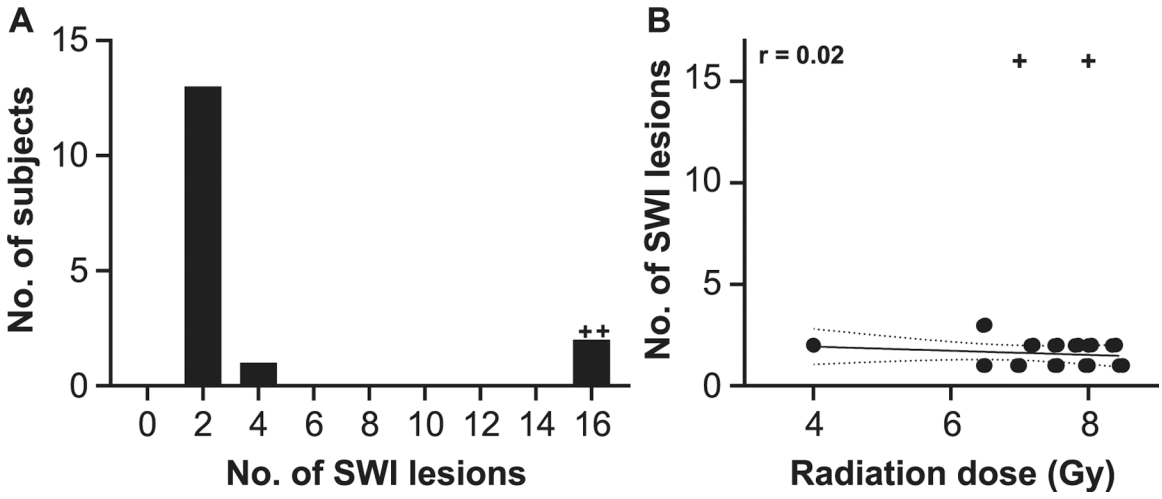

FIG. 4.

Evaluation of radiation-dose response on SWI-MRI lesion number. Panel A: Most animals had 1–2 SWI hypointense foci. Frequency histogram. Panel B: There was no statistically significant relationship between radiation dose and lesion number. Linear regression analysis, r = 0.2, $P > 0.05$. Solid line indicates best fit; slope = −0.1. Dotted lines indicate 95% confidence interval. $^{+}$Outlier, as determined by ROUT method and excluded from regression analysis.

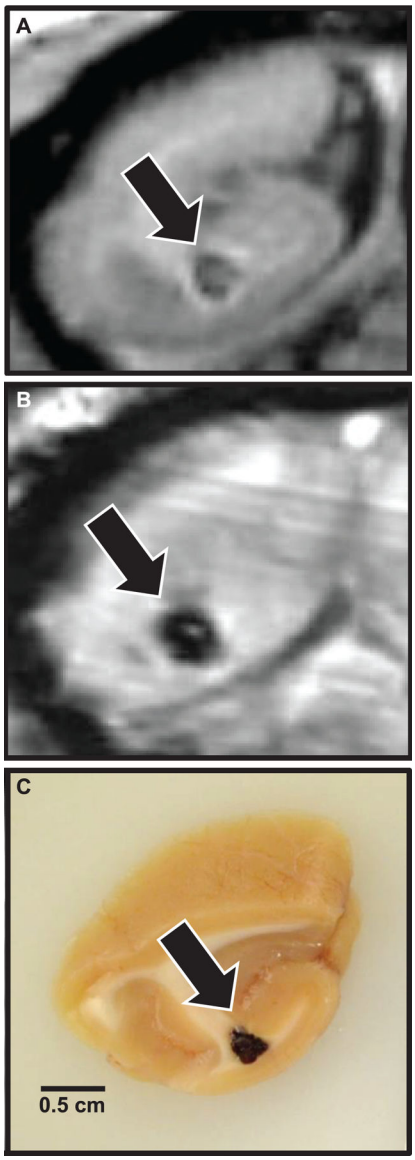

FIG. 5.

Localization of MRI lesions and correlative gross pathology. Coronal sections, occipital lobe, example of a focal brain lesion first noted six years postirradiation, at the time the first MRI scan was completed. Panel A: T1 MRI indicating focal parenchymal loss with central T1 isointense heterogeneity. Panel B: SWI-MRI indicating the presence of iron or calcium (blood or necrosis, respectively). Panel C: Gross tissue, demonstrating focal hemorrhage on sectioned surface.

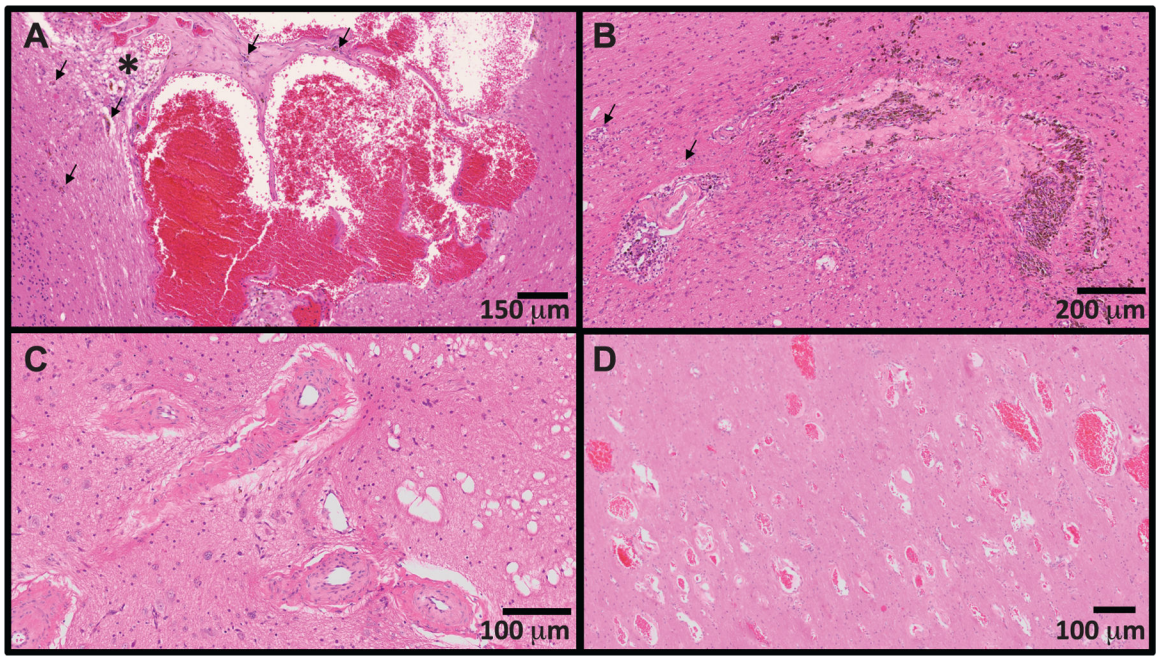

FIG. 6.

Spectrum of cerebrovascular injury observed in long-term survivors of TBI. Panel A: Dilated and malformed vasculature forming anastomosing channels (cavernous hemangioma). There are scattered hemosiderin-laden macrophages within the vascular wall and adjacent parenchyma (evidence of chronic hemorrhage; black arrows). The adjacent parenchyma is focally edematous (asterisk). Panel B: Transmural replacement of the vascular wall by extracellular matrix with chronic hemorrhage and occlusion of the vascular lumen. Recanalization (small caliber capillaries distributed throughout the occluded lumen) and aggregates of hemosiderin-laden macrophages (brown pigment, hemorrhage) are indicative of chronic injury. The adjacent parenchyma is infiltrated by increased numbers of astrocytes and elongated, activated (reactive) microglia (rodcells). There is degeneration of the cerebral peduncle (swollen axons, dilated myelin sheathes, digestion chambers; black arrows). Panel C: Tortuous and redundant vasculature dissecting through the left optic tract with marked thickening (5x normal thickness) of the tunica media by extracellular matrix and smooth muscle hyperplasia. There is scattered vacuolation of the adjacent optic tract. Panel D: Widespread infiltration of the deep occipital white matter by abnormally dilated and haphazardly arranged capillaries (telangiectasia). The lesion was an incidental finding, and not present on susceptibility-weighted imaging six months prior to necropsy.

TABLE 1

Subject Demographics

	Nonirradiated	Irradiated NSL	Irradiated SWI
n	53	104	16
Males (n)	50	79	12
Females (n)	3	25	4
Age at assessment (years)	6.2 (3.5–18.3)	6.5 (2.8–16.5)	7.2 (4.3–9.8)
Age at irradiation (years)	-	4.3 (2.3–15.3)	3.8 (3.0–6.7)
Dose (Gy)	-	6.6 (1.14–8.5)[a]	7.4 (4–8.5)[a]
Dose rate (Gy/min)	-	0.6 (0.6–0.8)	0.6 (0.6–0.8)
Irradiation-to-diagnosis interval (years)	-	-	1.0 (0.6–11.3)
Age at lesion diagnosis (years)	-	-	7.2 (4.3–14.7)

Notes. All data are presented as median (range). NSL = no significant lesions; SWI = susceptibility-weighted imaging (brain lesion).

[a] $P \leq 0.05$.

Author Manuscript

Author Manuscript

Author Manuscript

TABLE 2

Animals Receiving TBI are More Likely to Develop SWI Hypointense Lesions Detectable on MRI

	Control	TBI	Total
No lesions	53	104	157
Lesion(s)	0	16	16
Total	53	120	

Note. Fisher's exact test, $P = 0.003$.

TABLE 3

Neuroanatomic Distribution of SWI Hypointense Foci

	Gray matter	Gray/white junction	White matter	>Resolution of T1	Total
Frontal	0	2	3	5	10
Parietal	1	2	5	4	12
Temporal	0	0	1	0	1
Occipital	4	6	8	7	25
Internal capsule	0	0	1	0	1
Optic tract	0	0	1	0	1
Thalamus	1	1	0	1	3
Cerebellum	1	0	0	0	1
Brainstem and spinal cord	1	0	0	0	1
Total	8	11	19	17	55

TABLE 4

Demographics of Deceased Animals with SWI Hypointense Brain Lesions

	NHP1	NHP2
Dose (Gy)	7.2	7.6
Age at necropsy (years)	11.3	15.5
Age at irradiation (years)	3.4	3.0
Irradiation-death interval (years)	7.8	12.4
Irradiation-lesion-diagnosis interval (years)	5.8,[a] 7.3	6.8, 8.4

[a]Lesion present at the time of first MRI.